Functional Materials Letters
Vol. 7, No. 1 (2014) 1350068 (9 pages)

DOI: 10.1142/S1793604713500689

World Scientific
www.worldscientific.com

PROPERTIES OF A THREE-DIMENSIONALLY ORDERED MACRO-MESOPOROUS CARBON-DOPED TiO_2 COMPOSITE CATALYST

WUBIN SUI[*,†,**], JINGTANG ZHENG[†,**], CHARLES U. PITTMAN JR.[‡], NASR BENSALAH[§], MINGBO WU[†] and YUCUI ZHAO[†]

[*]*Department of Chemistry and Chemical Engineering*
Zaozhuang University, Zaozhuang 277160, P. R. China

[†]*The State Key Laboratory of Heavy Oil Processing*
China University of Petroleum, Qingdao 255666, P. R. China

[‡]*Department of Chemistry, Mississippi State University*
Mississippi State, MS 39762, USA

[§]*Department of Chemistry and Earth Sciences*
College of Arts and Science, Qatar University
P. O. Box 2713, Doha, Qatar

Received 19 January 2013; Accepted 9 September 2013; Published 5 November 2013

This study aimed to develop an effective, environmentally benign composite catalyst composed of carbon materials and titanium dioxide (TiO_2). Carbon-doped titanium dioxide (C–TiO_2) was prepared by coating TiO_2 onto macro-mesoporous carbon (MMC). The structure, morphology and surface chemistry states of the C–TiO_2 were characterized by XRD, TEM, XPS, UV-vis and FTIR. The photocatalytic activity of C–TiO_2 was evaluated based on the decomposition of an aqueous methyl orange solution in visible light. C–TiO_2 significantly improved photocatalytic activity. A possible mechanism for the improvement of the photocatalytic activity of C–TiO_2 in visible light was proposed. The results of the analysis suggested that MMC played key roles as the support, absorbent, location of photo-generated electron transfer, and carbon-doping source during methyl orange photodegradation.

Keywords: Macro-mesoporous carbon; titanium dioxide; carbon doping; photocatalysis; mechanism.

Photocatalysis has made significant developments over the past few decades as a result of greater understanding of photocatalyst surface characteristics. Photoinduced charge carriers can be used for a variety of catalytic applications. Therefore, photocatalysis is an attractive method particularly in the degradation of organic dye in wastewater. In various photocatalytic products, the selective formation of a desired photocatalyst remains imperative.

Titanium dioxide (TiO_2) is an important semiconductor.[1] Its use as a photocatalyst for many chemical reactions is one of its most important applications. One example involves the reaction of an organic dye in wastewater.[2] The TiO_2/ultraviolet (UV) catalytic system has been widely investigated, and its photocatalytic mechanism is generally attributed to the creation of a hole–electron pair upon UV irradiation.[3,4] The hole can migrate to the surface and react with an OH^- group or O_2 absorbed on the catalyst surface to produce a hydroxyl radical or a superoxide radical cation, respectively.[3,4] The highly active species generated at the catalyst surface can efficiently oxidize organic compounds. However, TiO_2 cannot be practically applied as a photocatalyst because approximately only 4% of solar radiation energy can effectively generate hole–electron pairs. This limitation is due to the large band gap energy (3.2 eV) of anatase.[5] Therefore, modifying or doping TiO_2 is essential so that it can be activated in a visible light wavelength range.[6–8]

Carbon materials have attracted significant attention because of their unique properties and widespread applications. Carbon materials have been widely used in catalysts,[9–11] coatings,[12] sensors,[13,14] separation adsorbents and chemical filters,[15,16] photonics,[17–21] microelectronics, electro-optics, environmental engineering, chromatographic stationary phases,[22–24] insulators, biomaterials, controlled-release materials, and nanolithographic templates for etching.[25,26] Multi-walled macro-mesoporous carbon (MMC) has been widely investigated

**Corresponding authors.

for use in modifying TiO_2,[27] and carbon doped-TiO_2 composites have been obtained by using the sol–gel method.[28] These composites have good adsorption properties, such as cooperative or synergistic adsorption, and catalytic effects. In this study, we developed a composite catalyst, 3DOM carbon-doped TiO_2, by using a photocatalyst.

Analytical grade reagents were used in the experiment. Tetrabutyltitanate ($Ti(OC_4H_9)_4$), ethanol (CH_3CH_2OH), aqueous acetic acid ($C_2H_4O_2$), and methyl orange (MO) were purchased from Shanghai Chemical Reagents Co. P25 TiO_2 from Degussa was employed as a standard photocatalyst for comparison with the prepared photocatalyst. P25 TiO_2 mainly consisted of anatase-phase (ca. 80%) non-porous polyhedral particles with a mean size of ca. 30 nm and a Brunauer–Emmett–Teller surface area of $45\,m^2g^{-1}$.

The C–TiO_2 system was prepared by using sol–gel method. Tetrabutyltitanate (TBT, 80 mmol) was used as the precursor in anhydrous ethanol (60 ml). Aqueous acetic acid (20 ml) was added to catalyze the reaction, and the ethanol/TBT solution was hydrolyzed by adding 18 mL of deionized water. Gels were formed and then aged for 2 h at 35°C. MMC materials with different pore sizes were then synthesized based on the method used by Kim.[29] The MMC was used as a supporting template and adsorbent. Up to 3 g of MMC were added to the aged TiO_2 gel, and the mixture was subjected to weak sonication for 30 min in a water solution. To generate the final C–TiO_2 material, the samples were dried at 80°C for 3 h followed by calcination at 200°C for 2 h and then further calcined at 450°C for 2 h.

The crystalline structure of the samples was determined by using X-ray diffraction performed with a Philips X'Pert MPD Pro X-ray diffractometer with Cu-Ka radiation ($\lambda =$ 1.5406 Å). Data were collected over 2θ values from 20° to 80° at a scan speed of 1°/min. D is the crystal size, which was calculated by using Scherrer's equation $D = \frac{K}{B\cos\theta B}$, with $\lambda = 1.54178$ Å and $K = 0.89$, and B is the length in radians at half the peak's intensity with diffraction angle B. The surface properties of the samples were examined by using X-ray photoelectron spectroscopy (XPS) on a Kratos AXIS Ultra DLD system which employs monochromatic Mg-Ka excitation. All the bonding energies were calibrated by using the C 1s level at 284.8 eV as an internal standard peak. Gatan ORIUS™ SC 200CCD was used for transmission electron microscopy (TEM) to examine the product microstructure. Ultraviolet-visible (UV-vis) diffuse reflectance spectra were obtained by using a Perkin Elmer Lambda 750S UV/Vis spectrophotometer equipped with an integrating sphere assembly. The spectra were recorded at room temperature in air from 300 nm to 800 nm. The Fourier transform infrared spectroscopy(FTIR) were obtained on a spectrophotometer (Nicolet 6700).

To confirm the performance of the catalyst, MO degradation in the as-prepared catalyst samples was investigated. First, MO adsorption was studied by using a homemade quartz photochemical reactor (Fig. 1) in the dark. The reactor, which contains 1 g of C–TiO_2 adsorbent and 500 mL of MO solution at a concentration of 40 mg/l (C_0), was prepared. Air was bubbled through the adsorption tubes, which caused the formation of a homogenous suspension of the C–TiO_2 adsorbent in the solution. The suspension was continuously stirred magnetically at 20°C in the dark to ensure that the mixture reached adsorption equilibrium on the catalyst surface. Samples were taken at different time intervals and filtered by using a Millipore Millex 25 0.45 μm membrane filter. The MO concentration in the remaining clear liquid (C_t) was measured by using UV-vis spectroscopy.

MO degradation was carried out in a reactor (Fig. 1) fitted with a circulating water cooling system to maintain constant temperature. A medium-pressure 500 W Xenon vapor lamp was used for visible light irradiation, and the UV light source was a 500 W mercury lamp. Air was bubbled through the reaction in all experiments to provide oxygen for oxidation, thereby causing the formation of a homogenous suspension of the catalyst in the solution. The initial concentration of the MO solution in all experiments was 40 mg/l (C_0). Before illumination, the suspension was magnetically stirred for 30 min in the dark to ensure that the mixture reached adsorption equilibrium on the catalyst surface. During photoreaction, 10 mL of the solution was removed every 10 min. Next, the photocatalyst was separated from the solution by centrifugation and then filtered by using a Millipore Millex 25 0.45 μm membrane filter. The MO concentration in the

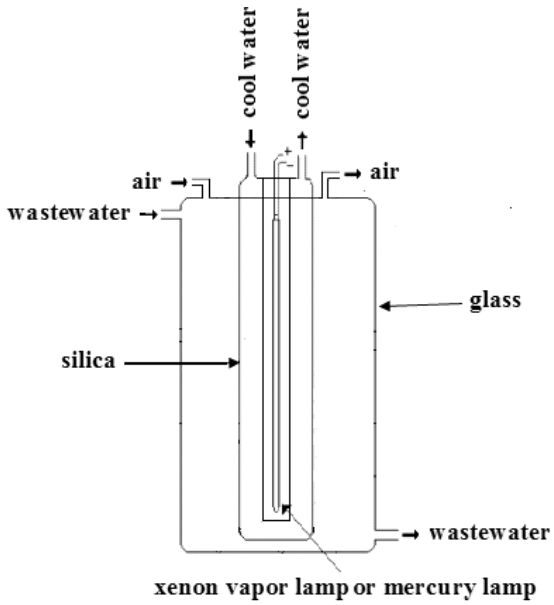

Fig. 1. Photocatalytic reactor.

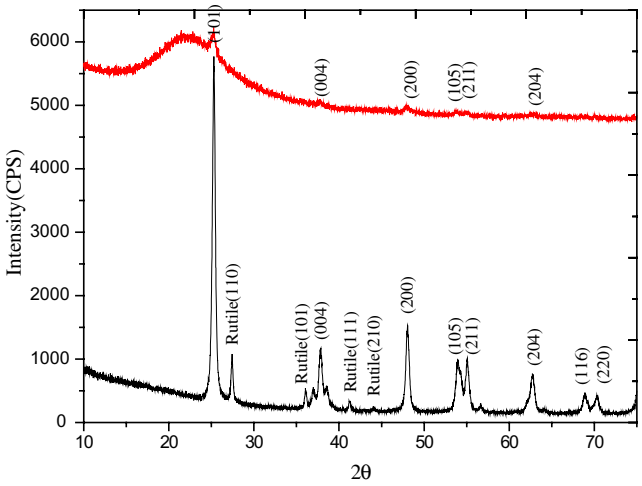

Fig. 2. XRD patterns of (a) TiO_2 and (b) carbon-doped TiO_2.

remaining clear liquid (C_t) was measured by using UV-vis spectroscopy.

The X-ray diffraction patterns of the pristine C–TiO_2 and the pure (undoped) TiO_2 synthesized by using sol–gel condensation are shown in Fig. 2. The 2θ diffraction peaks of pure TiO_2 (a) at 25.3°, 37.8°, 48.0°, 53.9°, 55.1° and 62.8° correspond to the diffraction peaks of the (1 0 1), (0 0 4), (2 0 0), (1 0 5), (2 1 1) and (2 0 4) crystal planes of anatase TiO_2, respectively. The peak at 27.4° was for rutile TiO_2. This 27.4° diffraction peak disappeared in the C–TiO_2 (b) sample which exhibited typical anatase-type TiO_2 peaks only. C–TiO_2 was used to ensure that only the formation of anatase-type TiO_2 occurred without any other crystal forms. After calcination at 450°C, the rutile crystals transformed into anatase. Speculation about the reason is that carbon has a significant anatase crystalline phase stability, which limited crystal growth and grain sintering. In addition, the high potential energy surface, which was filled with macro-, meso- and microporous crystals, inhibited the phase transition of crystalline anatase. The interaction mechanism of carbon and TiO_2 in high temperature during carbonization was studied.

TEM was performed to investigate the morphology of the photocatalysts. Figure 3 illustrates the C–TiO_2 surface morphology. Many TiO_2 nanoparticles as well as a cluster of TiO_2 particles are present on the carbon surface [Fig. 3(a)]. The TiO_2 particles measure about 5 nm to 14 nm. The supported TiO_2 particles have a small size distribution, as seen in Fig. 3(a) and more clearly in Fig. 3(b). This finding indicates that ultrasonication promoted the dispersion of TiO_2 particles, and calcining maintained this size distribution during the loading process. After several ultrasonication cycles, TiO_2 nanocrystals aggregated on the carbon surface [Fig. 3(b)], which suggests that the MMC structure facilitated TiO_2 dispersion on the carbon surface after the formation of sol–gel TiO_2. The HRTEM images shown in Fig. 3(c) indicated that the crystal interplanar spacing (d-spacing) of the nanoparticle is about 0.35 nm, which is corresponding to the (1 0 1) planes of anatase TiO_2. The SAED pattern [inset of Fig. 3(c)] of this sample revealed a set of spots and rings, which can be indexed to (1 0 1), (0 0 4), (2 0 0), (1 0 5) crystal planes of anatase TiO_2. It is clearly seen that it is in good agreement with the XRD results.

XPS is a powerful method that is used to determine the electron structure of the valence states, oxidation states and chemical environment of atoms in the surface regions of solid materials. The survey XPS spectrum [Fig. 4(a)] shows that titanium, oxygen and carbon are present in the surface region of the carbon-doped TiO_2. Individual XPS C1s, O1s and Ti2p spectra were measured at a high resolution, as shown in

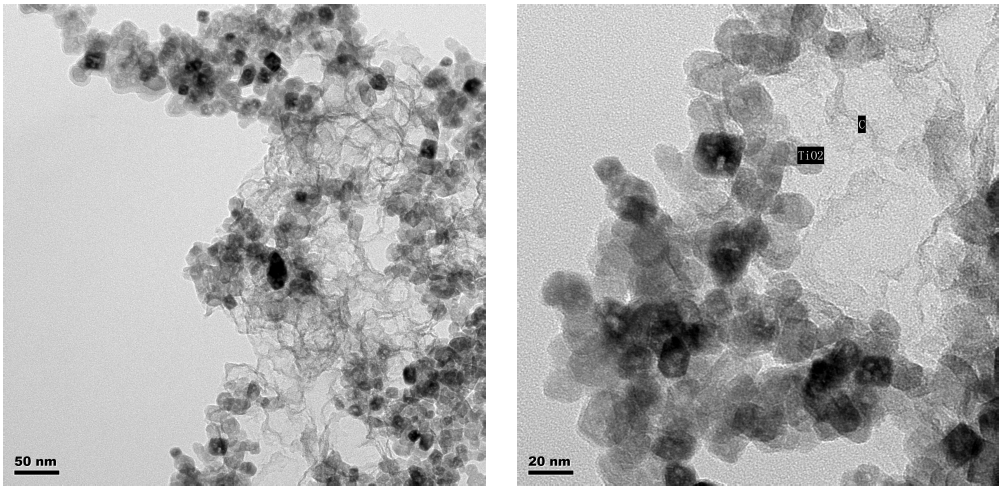

(a) (b)

Fig. 3. TEM images of carbon-doped TiO_2 photocatalysts (a) scale bar 50 nm, (b) scale bar 20 nm, (c) HRTEM micrographs and SAED patterns.

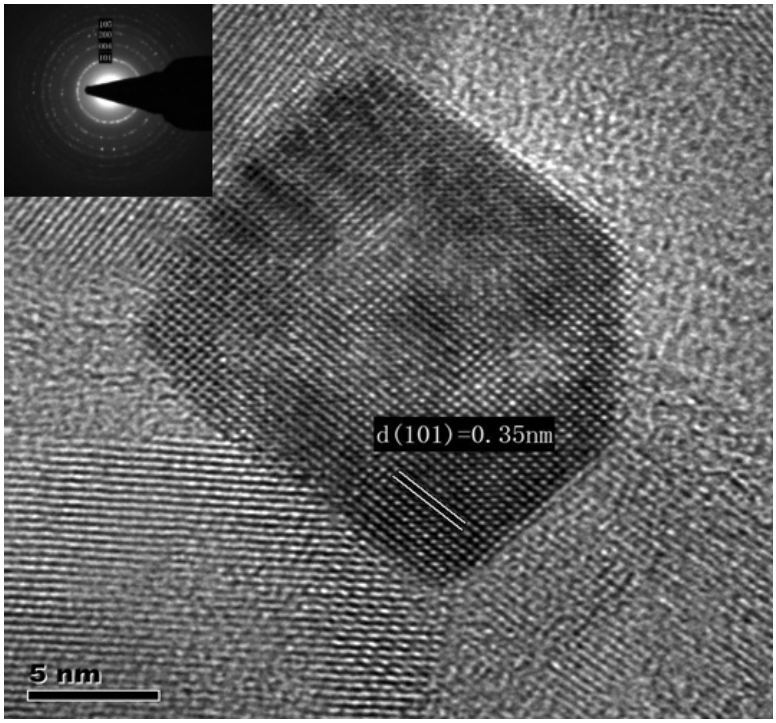

(c)

Fig. 3. (*Continued*)

Figs. 4(b)–4(d). The high-resolution C1s XPS spectrum in Fig. 4(b) showed four peaks at respective binding energies of approximately 284.4, 286.0, 287.5 and 289.0 eV. The major peak with a binding energy of 284.4 eV corresponds to graphitic carbon from MMC. The 286.0 eV peak is ascribed to highly oxidized carbon. This result is consistent with carbon bonded to a single oxygen bond. Thus, it is assigned to a C–O– Ti≡bonded carbon when TiO_2 has chemically united with carbon at the calcined MMC surface. This phenomenon keeps TiO_2 fixed on the surface of the carbon C–TiO_2. The other peaks with binding energies of 287.5 eV and 289.0 eV correspond to C=O and –COOH.[30] The XPS spectra of the O1s spectrum in Fig. 4(c) consist of three peaks. The peaks at 528.9, 530.3 and 531.2 eV are ascribed to Ti-O bonds,[31] Ti-OH bonds (hydroxyl groups), and C–O (Ti–O–C) bonds, respectively, in agreement with the C1s spectrum. The chemisorbed OH^- on the surface of TiO_2 can react with the trapped hole to improve the activity of the photocatalyst.[32]

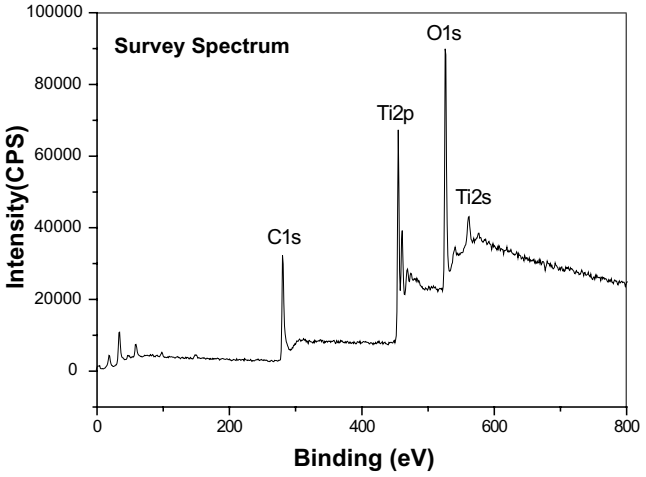

(a)

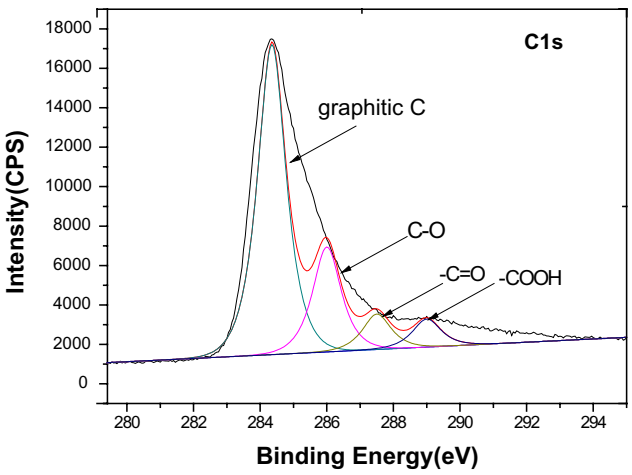

(b)

Fig. 4. XPS spectra of (a) survey spectrum, (b) C1s, (c) O1s and (d) Ti2p in the C–TiO_2.

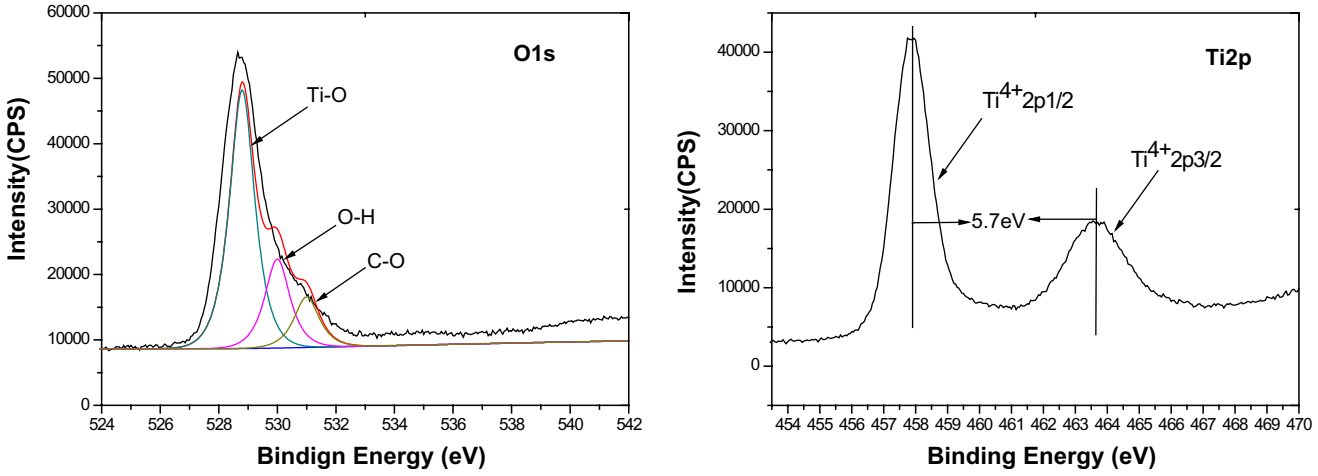

(c) (d)

Fig. 4. (*Continued*)

The Ti–O–C bond is a result of the close contact and reaction of TiO_2 nanoparticles with MMCs at higher temperature.[33,34] The two lower binding energy peaks of the O1s spectrum indicate a change in the chemical environment of the hybrid composite surface. These changes could be related to the improved visible light photocatalytic activity of C–TiO_2. The Ti2p spectra in Fig. 4(d) contain two peaks located at binding energies of 463.6 eV and 457.9 eV. These peaks are assigned to Ti^{4+} 2p3/2 and Ti^{4+} 2p1/2, respectively. The binding energies are lower than those of the typical Ti 2p signal of Ti^{4+} (458.7 eV and 464.4 eV), which indicates that the chemical environment of Ti in C–TiO_2 differs from that of pure anatase.[34] This result may be due to the somewhat lower oxidation state of titanium when surrounded by both carbon and oxygen atoms.[35]

The distribution of functional groups on the surface of composite photocatalyst indicates that some parts of the surface of carbon were exposed when TiO_2 burned off after high-temperature calcination. After high-temperature sintering, the oxygen functional groups and active carbon atoms on the surface of the composite photocatalyst chemically bonded or cross-linked to produce the C–O–Ti≡chemical bond.[36]

Unsaturated dangling bonds formed on the carbon atoms on the edge of the graphite layers of the composite photocatalyst because the chemical bonds were interrupted, which enhanced the adsorption of negatively charged oxygen atoms or association, thus strengthening the chemical adsorption of electropositive hydroxyl (–OH) hydrogen atoms because of TiO_2. The increased surface charge may reduce the band gap energy of the semiconductor oxide.

The UV-vis absorption spectra of C–TiO_2 and pure TiO_2 are presented in Fig. 5. The sharp absorption edge of C–TiO_2 is greater than that of pure TiO_2 in the UV-vis range. The high UV irradiation absorption of C–TiO_2 is due to the presence of photosensitive functional groups on the surface of these materials, which indicates that this sample should behave as a UV-photosensitive material.[37] Nevertheless, C–TiO_2 has strong absorption throughout the entire visible light region. This absorption is stronger than that of pure TiO_2 because the carbons at the interstitial positions of TiO_2 lattice induce several localized occupied states in the gap, which contribute to the red shift of the absorption edge toward the visible light region.[38]

The spectrum of the C–TiO_2 sample shows a steep absorption edge at about 410 nm and a wide absorption shoulder band in the range of 400 nm to 800 nm, which indicates that a larger fraction of visible light could be absorbed to induce electron–hole pairs.[39] This finding shows

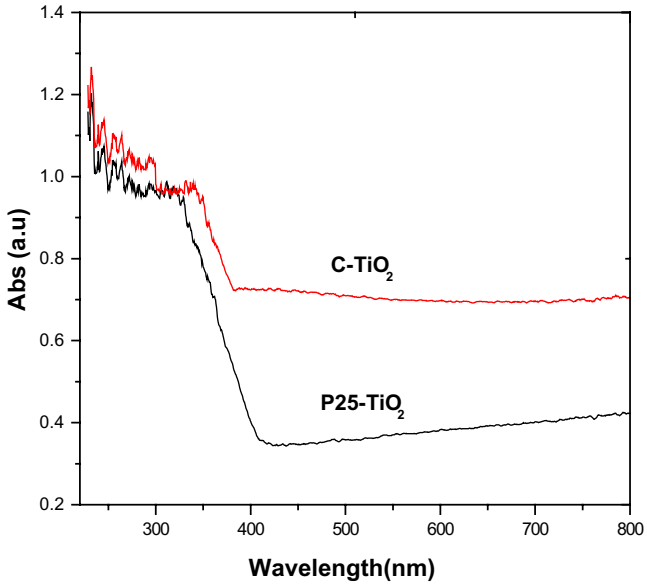

Fig. 5. UV–vis absorption spectra of (a) TiO_2 and (b) carbon-doped TiO_2.

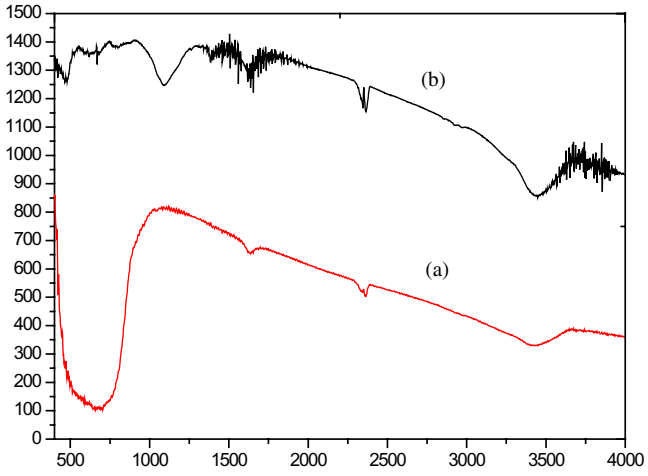

Fig. 6. FTIR spectra of (a) P25–TiO_2 (b) C–TiO_2.

that C–TiO_2 may act as a photocatalyst under visible light irradiation if this greater visible light absorption can induce hole pair separation.[40]

Infrared (IR) spectroscopy can detect the molecular rotational and vibrational energy levels, which establish the functional group and bonding state on the surface of the material. The extinction coefficient of the carbon material is close to that of graphite, which has a strong IR radiation absorption. However, the pass rough surface will lead to IR light scattering. To overcome interference in the functional group discrimination, we use the surface DRIFT technique to explore the organic groups of information on the surface of the composite photocatalyst.

The IR spectra of the composite photocatalyst show that the broad absorption peak near 3431 cm^{-1} is caused by hydroxyl (OH) stretching vibration, which indicates the presence of an OH^- group produced by the composite photocatalyst surface adsorption of water and pore water. The absorption peaks near 1580 cm^{-1} and 1610 cm^{-1} correspond to the fused-ring aromatic carbon–carbon double-bond skeleton stretching vibration. However, most researchers attribute this peak to carboxyl (COO–) stretching vibration, which is consistent with the results of the XPS spectrum. The absorption peak near 1510 cm^{-1} is a benzene ring structure. The sharp peaks near 1610 cm^{-1} and 1507 cm^{-1} are produced by the aromatic ring, and the acromion near 1720 cm^{-1} to 1667 cm^{-1} is caused by the conjugate action of –C=O and –C=C–.[41] The broad absorption band in 1500 cm^{-1} to 1750 cm^{-1} is composed of several overlapping absorption peaks.

The absorption peak near 1370 cm^{-1} is attributed to =C–H plane rocking. The absorption peaks near 1220 cm^{-1} and 1240 cm^{-1} are possibly produced by the CO asymmetric stretching vibration in the ether bond. The strong absorption near 1020 cm^{-1} is attributed to the asymmetric stretching vibration of transitional-state carbide (Ti–C–) bond and the generation of hybrid polymerization Ti–O–C during hydrolysis and its attachment to the surface of the TiO_2 particles; these particles have good thermal stability because they require a higher energy to bond cleavage. This inference is consistent with the result of the XPS spectrum on the composite photocatalyst.

The strong, broadly split absorption bands in the short wave near 500 cm^{-1} to 720 cm^{-1} are caused by the vibration of the Ti–O–Ti bond, Which is the typical anatase structure.

Therefore, the functional groups on the surface of C–TiO_2 are aromatic ring, hydroxyl, carboxyl, and other oxygen-containing groups produced by high-temperature calcinations.

Characterizations of the aforementioned samples indicate that the surface layer of C–TiO_2 is not simply due to the UV and visible light wave that acts as a physical barrier and affects the semiconductor's absorption of effective light wave. The surface layer is also ascribed to the presence of surface functional groups that change the charge distribution of the oxide surface, the absorption band edge, and the apparent absorbance. These functional groups significantly weaken the oxidation-reduction potential and eventually lead to the transport of photogenerated electrons and migration of holes to the catalyst surface.

MO is a very stable and common dye that is extensively used in various industrial applications.[41] Therefore, many studies have employed MO as a model pollutant to evaluate the efficiency of TiO_2-mediated photocatalysis.[42–44]

To estimate the photocatalytic activity of C–TiO_2, we investigated the decolorization of MO in a solution under UV [Fig. 7] and visible light irradiation ($\lambda > 420$ nm) [Fig. 8] at a

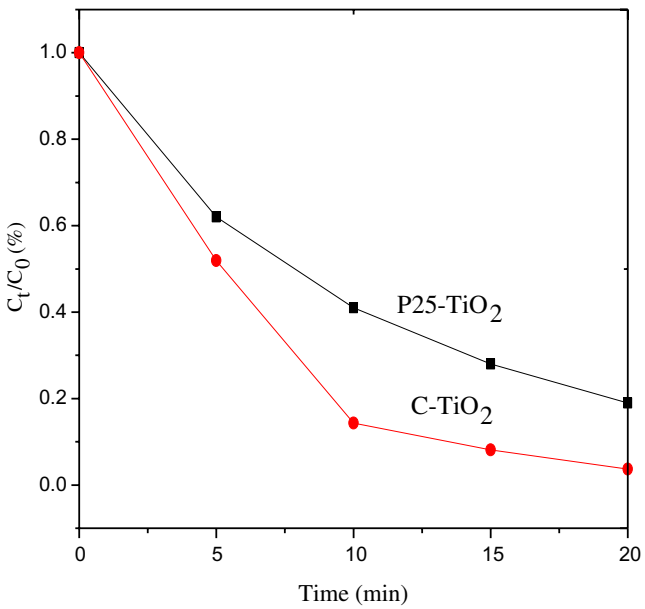

Fig. 7. Decolorization rate MO on P25–TiO_2 and MMC–TiO_2 in UV (C_0 is the initial concentration of MO; C_t is the concentration of MO at time t).

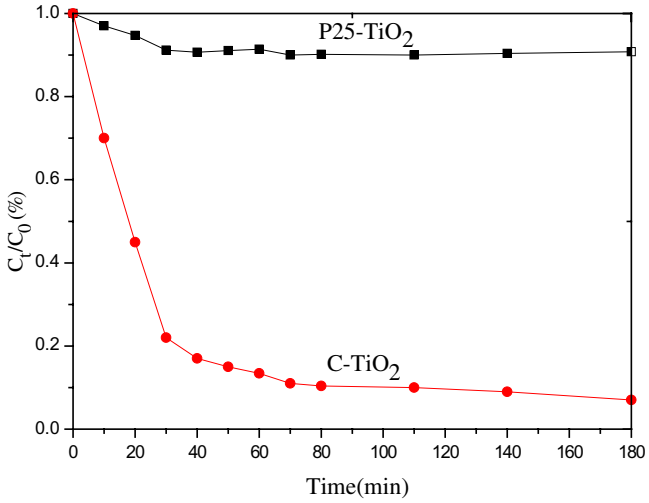

Fig. 8. Decolorization rate at 20° C MO on P25–TiO_2 and MMC–TiO_2 in Vis (C_0 is the initial concentration of MO; C_t is the concentration of MO at time t).

certain time. For comparison, the efficiency of P25 TiO_2 is examined under the same experiment conditions. As shown in Fig. 7, C–TiO_2 catalysts are more efficient than P25 TiO_2 in the presence of UV light. This efficiency can be ascribed to the presence of carbon substrates, which improved the photoelectron and electron–hole separation of the supported TiO_2. Figure 8 shows the activity of C–TiO_2 catalysts in the presence of visible light ($\lambda > 420$ nm). P25 has relatively poor photocatalytic activity due to its limited photoresponse range. Compared with the efficiency of P25, the composite C–TiO_2 exhibits faster decoloration.

The MO adsorption capability of C–TiO_2 and P25 TiO_2 was also evaluated by conducting experiments under the same conditions without irradiation [Fig. 9]. Adsorption equilibriums were achieved within 30 min. Composite C–TiO_2 provided MO with superior adsorption capability compared with P25–TiO_2, which is in agreement with the faster photocatalytic decomposition of MO over C–TiO_2. The large adsorption capacity can promote the organic decomposition efficiency of C–TiO_2 under visible light.[44] Although the visible light cannot directly excite valence band electrons to the conduction band of TiO_2, electrons can jump to the conduction band through thermal excitation or energy transfer from the excitations in the visible light absorption by the carbon layer. Conduction band electrons will quickly recombine with holes.[45] Aside from being a substrate adsorbent and a sensitizer in visible light, carbon can also serve as an electron scavenger to inhibit the recombination of the photogenerated carriers.[44] In this work, the C–TiO_2 composites provide better MO adsorption which may help transfer MO molecules to the TiO_2 surface. Thus, the C–TiO_2 composites have superior adsorption and higher photocatalytic activities which promote photodegradation efficiency because of the synergistic effect of carbon substrate and titanium.

The intermediates and the photodegradation mechanism of MO in visible light were identified through high-performance liquid chromatography-tandem mass spectrometry (HPLC-MS). The HPLC profiles (Fig. 10) recorded at 465 nm correspond to MO solutions degraded at 0 and 15 min. After 15 min of irradiation, three new peaks are clearly observed, except for the peak that corresponds to MO. By analyzing the samples of the three new peaks through HPLC-MS, three fragments with m/z values of 353, 320 and

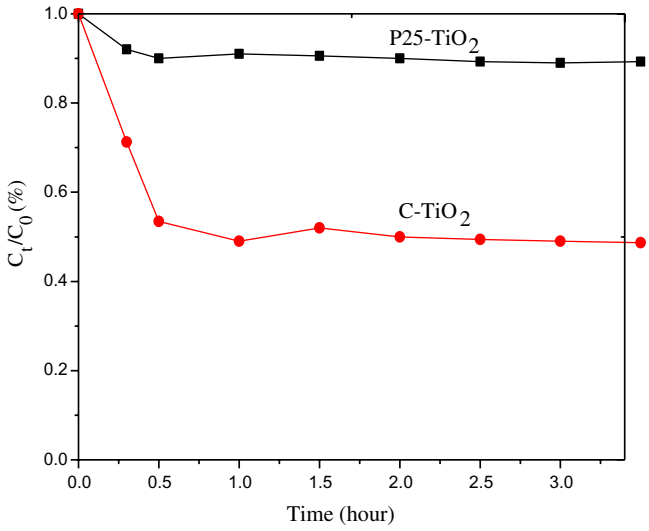

Fig. 9. Adsorption of methyl orange from water over P25–TiO_2 and C–TiO_2 in the dark (C_0 is the initial concentration of MO; C_t is the concentration of MO at time t).

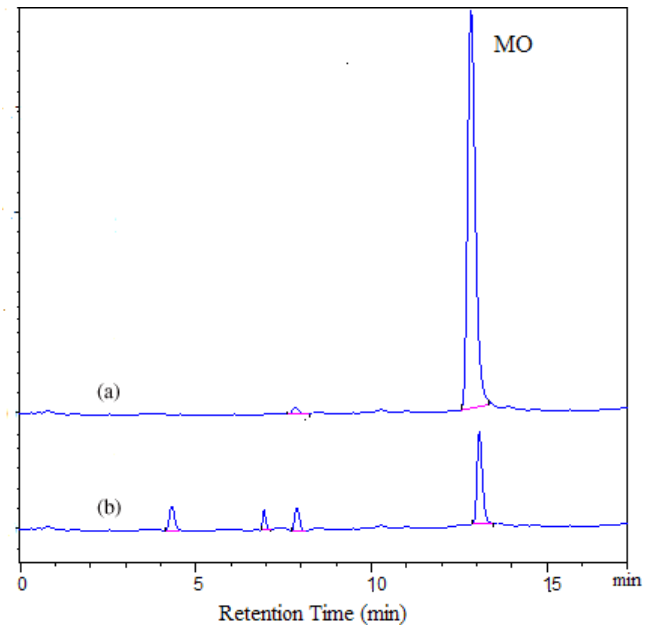

Fig. 10. HPLC of samples MO (a) MO solution, (b) MO solution degraded 15 min.

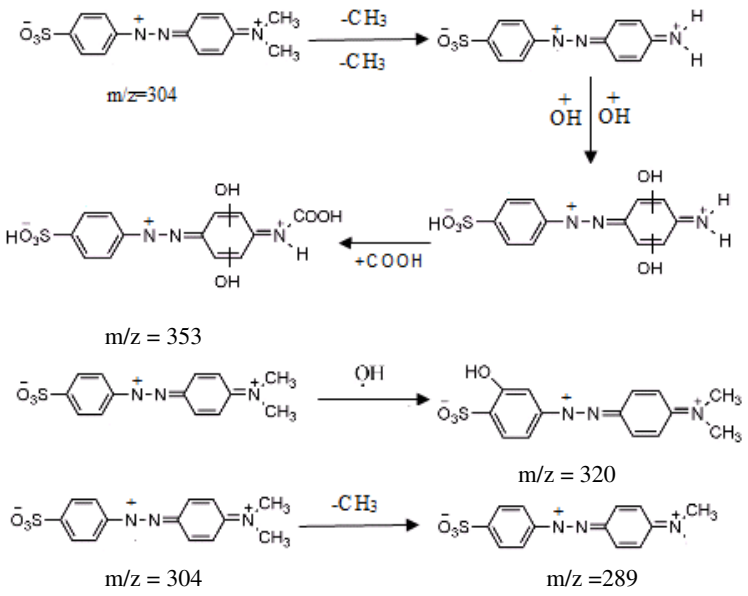

Fig. 11. Proposed photodegradation pathways for the intermediate.

289 were observed. Figure 11 shows the numerical agreement between the molecular weights and the hypothesis of the formation mechanism. This result indicates that MO is degraded under visible light irradiation.

A C–TiO_2 photocatalyst with superior performance to TiO_2 in MO photodegradation was successfully prepared. Its structure, surface morphology and surface oxidation states were investigated. XPS spectra indicated that titanium is chemically linked to its carbon support through the formation of ≡Ti–O–C chemical linkages during the preparation of the C–TiO_2 photocatalyst. The strong binding interaction between carbon and TiO_2 extends the photoresponse into the visible light range and enhances photogenerated charge separation and mobility properties. Simultaneously, the localized occupied states in the porous structure of carbon may restrict hole–electron recombination. In summary, C–TiO_2 is a better catalyst than P25–TiO_2 for the photodegradation of aqueous MO dye under UV and visible light irradiation. Therefore, this work may be important to the preparation of higher-performance TiO_2 photocatalysts and may facilitate an understanding of how such catalysts work.

Acknowledgments

This work was supported by the National Science Foundation of China (21176260, 20776159), the National Science Foundation of Shandong Province (ZR2009FL028), the Fundamental Research Funds for the Central Universities (09CX05009A), Program for New Century Excellent Talents in University, China Ministry of Education, 2009 (No. NCET-10-0768), the National Natural Science Foundation of China (Nos. 20876176, 51172285) and the Scientific and Technological Project of Zaozhuang (201129). The authors are grateful to the reviewers for their valuable suggestions and English corrections for the paper.

References

1. C. S. Turchi, D. F. Ollis, *J. Catal.* **122**, 178 (1990).
2. C. Minero, E. Pelizzetti, S. Malato and J. Blanco, *Sol. Energy* **56**, 421 (1996).
3. O. M. Alfano, M. I. Cabrera and A. E. Cassano, *J. Catal.* **172**, 370 (1997).
4. K. Chhor, J. F. Bocquet and C. Colbeau-Justin, *Mater. Chem. Phys.* **86**, 123 (2004).
5. M. Schiavello, *Electrochim. Acta* **38**, 11 (1993).
6. N. G. Park, J. van de Lagemaat and A. J. Frank, *J. Phys. Chem.* **104**, 8989 (2000).
7. S. Cherian and C. C. Wamser, *J. Phys. Chem. B* **104**, 3624 (2000).
8. A. Zaban and Y. Diamant, *J. Phys. Chem. B* **104**, 10043 (2000).
9. P. T. Tanev, M. Chibwe and T. J. Pinnavaia, *Nature* **368**, 321 (1994).
10. A. Corma and M. E. Davis, *Chem. Phys. Chem.* **5**, 304 (2004).
11. M. E. Davis, *Nature* **417**, 813 (2002).
12. H. Yabu, M. Takebayashi, M. Tanaka and M. Shimomura, *Langmuir* **21**, 3235 (2005).
13. D. Van Noort, R. Rani and C. F. Mandenius, *Mikrochim. Acta* **136**, 49 (2001).
14. D. Van Noort and C. F. Mandenius, *Biosens. Bioelectron.* **15**, 203 (2000).
15. D. B. Akolekar, A. R. Hind and S. K. Bhargava, *J. Colloid Interface Sci.* **199**, 92 (1998).
16. K. Lewandowski, P. Murer, F. Svec and J. M. J. Frechet, *Anal Chem.* **70**, 1629 (1998).

17. J. D. Joannopoulos, R. D. Meade and J. N. Winn, Photonic Crystals: Molding the Flow of Light (Princeton University Press, 1995).
18. Y. N. X. Younan, B. Gates, Y. D. Yin and Y. Lu, *Adv. Mater.* **12**, 693 (2000).
19. P. S. J. Russell, J. D. Joannopoulos, R. D. Meade and J. N. Winn, *Nature* **381**, 290 (1996).
20. A. Urbas, R. Sharp, Y. Fink, E. L. Thomas, M. Xenidou and L. J. Fetters, *Adv. Mater.* **12**, 812 (2000).
21. M. Campbell, D. N. Sharp, M. T. Harrison, R. G. Denning and A. J. Turberfield, *Nature* **404**, 53 (2000).
22. S. F. Xie, F. Svec and J. M. J. Frechet, *J. Chromatogr. A* **775**, 65 (1997).
23. M. B. Tennikov, N. V. Gazdina, T. B. Tennikova and F. Svec, *J. Chromatogr. A* **798**, 55 (1998).
24. A. Palm and M. V. Novotny, *Anal. Chem.* **69** (1997) 4499–4507.
25. P. Mansky, C. K. Harrison, P. M. Chaikin, R. A. Register and N. Yao, *Appl. Phys. Lett.* **68**, 2586 (1996).
26. M. Park, C. Harrison, P. M. Chaikin, R. A. Register and D. H. Adamson, *Science* **276**, 1401 (1997).
27. M. Inagaki, *Solid State Ion.* **86–88**, 833 (1996).
28. S. U. M. Khan, M. Al-Shahry and W. B. Ingler Jr., *Science* **297**, 2243 (2002).
29. P. Kim, J. B. Joo, W. Kim, S. K. Kang, I. K. Song and J. Yi, *Carbon* **44**, 381 (2006).
30. C. Kozlowski and P. M. A. Sherwood, *Carbon* **24**(3), 357 (1986).
31. P. Górska, A. Zaleska, E. Kowalska, T. Klimczuk, J. W. Sobczak, E. Skwarek, W. Janusz and J. Hupka, *Appl. Catal. B* **84**, 440 (2008).
32. C. Chen, P. Lei, H. Ji, W. Ma and J. Zhao, *Environ. Sci. Technol.* **38**, 329 (2004).
33. G. An, W. Ma, Z. Sun, Z. Liu, B. Han, S. Miao, Z. Miao and K. Ding, *Carbon* **45**, 1795 (2007).
34. Z. Song, J. Hrbek and R. Osgood, *Nano Lett.* **5**, 1327 (2005).
35. D. E. Gu, Y. Liu, B. C. Yang and Y. D. Hu, *Chem. Commun.* **21**, 2453 (2008).
36. Y. Rusheng, Ph.D. Dissertation, *Preparation of the Composite Photocatalysts with Nano-sized TiO_2 and Activated Carbon Fibers and Their Photocatalytic Properties*, Institute of Coal Chemistry Chinese Academy of Sciences, 2005.
37. X. Wang, S. Meng, X. Zhang, H. Wang, W. Zhong and Q. Du, *Chem. Chem. Phys. Lett.* **444**, 292 (2007).
38. H. Li, D. Wang, H. Fan, P. Wang, T. Jiang and T. Xie, *J. Colloid Interface Sci.* **354**, 175 (2011).
39. A. Lua, Y. Lia, M. Lva, C. Wanga, L. Yanga, J. Liua, Y. Wang, K.-H. Wongd and P.-K. Wong, *Sol. Energy Mater. Sol. Cells* **91**, 1849 (2007).
40. S. Sakthivel and H. Kisch, *Angew. Chem., Int. Ed.* **42**, 4908 (2003); D. E. Gu, Y. Liu, B.C. Yang and Y. D. Hu, *Chem. Commun.* **21**, 2453 (2008); C. D. Valentin, G. Pacchioni and A. Selloni, *Chem. Mater.* **17**, 6656 (2005).
41. S. Livraghi, M. C. Paganini, E. Giamello, A. Selloni, C. D. Valentin and G. Pacchioni, *J. Am. Chem. Soc.* **128**, 15666 (2006).
42. Y. Shen, T. Xiong, T. Li and K. Yang, *Appl. Catal. B* **83**, 177 (2008).
43. W. Han, P. Liu, R. Yuan, J. Wang, Z. Li, J. Zhuang and X. Fu, *J. Mater. Chem.* **19**, 6888 (2009).
44. T. Tsumura, N. Kojitani, I. Izumi, N. Iwashita, M. Toyoda and M. Inagaki, *J. Mater. Chem.* **12**, 1391 (2002).
45. M. Janus, M. Inagaki, B. Tryba, M. Toyoda and A. W. Morawski, *Appl. Catal. B* **63**, 272 (2006).
46. O. Akhavan, M. Abdolahad, Y. Abdi and S. Mohajerzadeh, *Carbon* **47**, 3280 (2009).
47. T. Xiao and Z. Jiang, UK Patent, WO 2008/009919 A1, 2008.